Atomic Layer Deposition of Lithium Borate and Lithium Borophosphate for Lithium-Ion Batteries

Reference

T. Verhelle, A. Dhara, L. Henderick, M. Minjauw, L. De Taeye, J. Meersschaut, J. Dendooven, C. Detavernier, Chemistry of Materials **37** (2), 687–696 (2025)

Full text (Publisher's DOI): doi.org/10.1021/acs.chemmater.4c02747

Atomic Layer Deposition of Lithium Borate and Lithium Borophosphate for Lithium-Ion Batteries

Tippi Verhelle,[†] Arpan Dhara,[†] Lowie Henderick,[†] Matthias Minjauw,[†] Louis De Taeye,[‡] Johan Meersschaut,[‡] Jolien Dendooven,[†] and Christophe Detavernier*,[†]

[†]*Department of Solid State Sciences, Ghent University, Krijgslaan 281 S1, 9000 Gent, Belgium*

[‡]*imec, Kapeldreef 75, B-3001 Heverlee, Belgium*

E-mail: Christophe.Detavernier@Ugent.be

Abstract

Protective coatings on lithium-ion battery electrodes have proven to be an effective way to suppress detrimental side reactions, thereby improving the performance of lithium-ion batteries. Atomic layer deposition (ALD) provides conformal deposition of these layers with precise thickness control, ensuring optimized cathode protection. In this work, an ALD process is developed for the deposition of lithium borate coatings using lithiumbis(trimethylsilyl)amide (LiHMDS), H_2O and trimethylborate (TMB). The ionic conductivity varies with deposition temperature: a value of 1.17 x 10^{-7} S cm^{-1} at 25°C is obtained, with an activation energy of 0.58 eV. Using a supercycle approach to combine lithium borate with the known Li_3PO_4 process, and varying the cycle ratio, allows for the deposition of borophosphate coatings with tunable B/P ratios. As-deposited Li_3PO_4 films are crystalline, whereas lithium borate films

are amorphous. Interestingly, a small amount of B incorporation ($<$ 1 at.%) enhances the crystallinity of the Li_3PO_4 films, which was attributed to a lower amount of C contamination (from 9.3 at.% to 4.4 at.%). To explore the electrochemical properties of these layers, 10 nm coatings were deposited on a $LiMn_2O_4$ electrode as a model 2D system, where good Li-kinetics were proven. Next to this, they have shown to provide protection at elevated potentials. This work demonstrates that lithium borate and lithium borophosphate coatings are promising materials for interfacial layers and solid-state electrolytes to be used in next-generation lithium battery technologies.

1 Introduction

Lithium-ion batteries (LiBs) are the leading battery technology in the energy storage market due to their superior energy density compared to other available battery technologies. However, the demand for higher energy densities and longer cycle life continues to drive research into addressing key degradation issues that occur during cycling. One challenge is degradation at the cathode interface, where side reactions such as transition metal dissolution and electrolyte oxidation lead to performance loss[1]. The latter process forms an unstable cathode-electrolyte interphase at high potentials, hindering ion transport and reducing the overall efficiency of the battery.

To mitigate these issues, protective coatings on the cathode surface have been used to form an artificial interphase layer. These interfacial layers have shown to be able to prevent direct contact between the electrolyte and the cathode, reducing side reactions and prolonging battery life. For these coatings to be effective, they must meet several criteria: (1) conformal coverage to ensure complete protection, (2) high ionic conductivity to maintain efficient ion transport, and (3) chemical and electrochemical stability at the high voltages typical of cathode materials[2].

Atomic layer deposition (ALD) is an ideal technique for creating such coatings, as it allows for conformal deposition over complex surfaces and precise thickness control, which ensures efficient Li-ion transport and minimizes the added mass. It is a deposition technique in which the electrode surface is sequentially exposed to a series of gasses, where each gas reacts in a self-limiting way. ALD has been successfully used to deposit various materials on cathodes, including, but not limited to, metal oxides[3,4], phosphates[5] and various lithium-containing compounds[2,6–10], showing improved performance of the battery systems. Lithium-containing films, in particular, are of interest due to their potential to enhance ionic conductivity while providing a stable interface. Among various Li-containing layers developed by the ALD technique, a lithium borate-like material, Li_3BO_3-Li_2CO_3[6], has demonstrated the highest ionic conductivity of 2.2 x 10^{-6} S/cm at 25°C. Although carbon incorporation improves the ionic conductivity, the presence of Li_2CO_3 will limit the electrochemical potential window, as Li_2CO_3 decomposes at higher potentials vs Li^+/Li[6].

Borates, in general, have gained attention due to their wide bandgap and ability to stabilize the cathode surface. They have been employed as electrolyte salts and additives[11] or as interfacial layers prepared using mixing techniques[12–14], enhancing the cyclability of batteries by reducing degradation at the cathode. Despite these advantages, the existing literature on ALD processes for borates is rather limited[15]. There is a need for a suitable ALD process and a fundamental understanding of the electrochemical properties of pure lithium borate films. Recently, B_2O_3 directly deposited via ALD on an $LiNi_{0.83}Co_{0.12}Mn_{0.05}O_2$ (NMC) cathode showed improved performance after annealing in oxygen atmosphere[16], further proving the potential of borates for LiB applications.

In addition to borates, lithium borophosphate materials are particularly intriguing due to the 'mixed network former effect', where physical properties, such as ionic conductivity,

exhibit a non-linear behavior as a function of the composition[17,18]. Phosphate materials typically show good electrochemical stability, but have a lower ionic conductivity than borates. However, the inclusion of borate into the phosphate matrix can significantly enhance the ionic conductivity, resulting in the observation of a conductivity maximum at specific borate-phosphate ratios. Optimization of the composition can be highly beneficial for designing artificial interphase layers[19]. ALD is well-suited for this, as two ALD processes can be combined using a supercycle approach[20], offering control over the composition by varying the cycle ratio, thereby tuning the electrochemical properties.

In this work, we present a new ALD process for the deposition of lithium borate films. By studying the influence of the deposition temperature, we aim to optimize the composition and ionic conductivity of these materials. Furthermore, we make use of a supercycle approach to integrate lithium phosphate into the deposition process, forming lithium borophosphate films with varying B/P ratios. These materials are then investigated as a potential interfacial layer in lithium-ion batteries by depositing them on $LiMn_2O_4$ electrodes[21] and studying their impact on the electrode performance and electrochemical stability.

2 Experimental

ALD was performed using a custom-built high-vacuum pump-type reactor, with a heating block that could go to 300°C, connected to an argon-filled glovebox. During depositions, a base pressure of 5 x 10^{-6} mbar was maintained. The lithiumbis(trimethylsilyl)amide (LiHMDS, $LiN(Si(CH_3)_3)_2$, 97%, Sigma-Aldrich) precursor was heated at 90°C, with the temperature of the delivery lines heated to 115°C to prevent condensation. Argon served as the carrier gas, pulsing the LiHMDS into the chamber at 1.2 x 10^{-2} mbar. Trimethylborate (TMB, $B(OCH_3)_3$, 98 %, Sigma-Aldrich) and H_2O were kept at room temperature, with a pressure of 5 x 10^{-3} mbar. The trimethylphosphate (TMP, $PO_4(CH_3)_3$, 97%, Sigma-Aldrich)

was heated to 48°C to achieve a pressure of 8 x 10^{-3} mbar inside the chamber. The deposition chamber walls were kept at 120°C. A standard pump time of 60 s for water was used.

Material characterization was performed using several techniques. In-situ spectroscopic ellipsometry measurements were conducted with a J.A. Woollam M-2000 ellipsometer to monitor thin film growth during ALD growth. The optical indices of the layers were fitted using a Cauchy model in the CompleteEase software (J.A. Woollam). The growth per cycle was determined by applying a linear fit to at least 20 data points obtained after reaching linear growth conditions. X-ray diffraction (XRD) was performed in Bragg-Brentano θ:θ geometry on a Bruker D8 diffractometer using Cu Kα radiation, to assess the crystallinity of the material. X-ray photoelectron spectroscopy (XPS) and elastic recoil detection (ERD) measurements were performed to analyze film composition. XPS was carried out on a Theta Probe XPS instrument using monochromatic Al Kα rays (15 kV, 70 W) focused to a 0.3 mm diameter spot and under an incidence angle of 30° with respect to the surface normal. The input lens of the concentric hemispherical analyser is at an angle of 50° with respect to the surface normal and accepts electrons over a wide angular range (20°-80° with respect to the surface normal). Depth profiling was done by etching the sample in an area of 4 mm^2 using Ar^+ ions (500 eV, 700 nA) under an incidence angle of 45°. No charge compensation was used as the substrates were sufficiently conductive. Survey scans were acquired at 200 eV pass energy with a 0.5 eV step size, and detail scans were acquired at 50 eV pass energy with a step size of 0.1 eV. Calibration for all spectra was performed using the CasaXPS software[22], positioning the adventitious C 1s peak at 284.6 eV. To perform the quantification and peak fitting, a Shirley background subtraction and a Gaussian/Lorentzian product function GL(30) line shape was used. The full width at half maximum (FWHM) for each component of the O 1s peak was constrained to <2.0 eV, and was kept constant across all components. ERD measurements for lithium borate deposited at 125°C and 250°C were performed using a 9.592 MeV $^{35}Cl^{4+}$ ion beam, with a scattering angle of 40° and a sample tilt of 20°. Other

samples were measured using a 8.013 MeV $^{35}Cl^{4+}$ ion beam, a scattering angle of 40° and a sample tilt of 15°.

Electrochemical characterization was performed with solid state cells and liquid cells with thin film planar electrodes as a model system. All electrochemical tests were performed in an argon-filled glovebox to which the samples were transported without air exposure. For solid state cell characterization, a Si/300 nm SiO_2/10 nm TiO_2/80 nm Pt - stack served as the planar substrate for ALD, with the Pt layer being deposited via physical vapor deposition (PVD). After ALD of 80 nm films and without air exposure, Pt dots of varying size where sputtered onto the samples using a mask, resulting in a metal-ALD film-metal structure. The prepared samples were mounted on a home-built stage, equipped with a heater. Impedance spectroscopy measurements were conducted with a commercial potentiostat (Metrohm Autolab PGSTAT302N). For liquid cell measurements, a home-built potentiostat[23] was connected to a three-electrode cell. A PTFE body filled with electrolyte (1M $LiClO_4$ in propylene carbonate (99.7%, Sigma-Aldrich)) was clamped against the planar working electrode. In addition to the above mentioned PVD Pt, coated $LiMn_2O_4$ films (a Si/300 nm SiO_2/10 nm TiO_2/100 nm PVD Pt/90 nm PVD $LiMn_2O_4$/coating - stack)[21] were used as electrodes, with the coated side pointing to the electrolyte. Electrical contact was ensured by connecting the bottom side of the electrode with copper foil using silver paste. The surface area of the exposed working electrode is 1.05 cm^2. Lithium strips were used as counter and reference electrodes.

3 Results and discussion

3.1 Lithium Borate Thin Films

3.1.1 Atomic layer deposition of lithium borates

In this work, we aimed to develop a new process based on the known lithium phosphate process, LiHMDS - TMP, as reported by Hämäläinen et al[24], where the direct combination of LiHMDS and TMP leads to the formation of Li_3PO_4. Due to the similarities between TMP and TMB as a precursor, a similar two-step process was initially attempted for the deposition of a pure lithium borate, but showed no visible growth, as can be seen in figure 1a) (black). This indicates that the reactivity between both the TMB and the LiHMDS is too low, and that an additional processing step is required to boost the reactivity. In this regard, pulsing an additional oxygen source is expected to hydroxylate the surface, providing the necessary -OH groups to enhance the surface reactivity towards the methoxy ligands of TMB[15]. In this work, the use of a water pulse between the LiHMDS and the TMB was preferred over an oxygen plasma or ozone, because in combination with LiHMDS the latter two can result in significant Si incorporation in the film due to the dual-source behavior of the LiHMDS precursor, shown by Werbrouck et al[25] and Tomczack et al[26]. Even in a three-step process, e.g. LiHMDS - O_2^* - TMP, 22 at.% of Si was incorporated in the film[25].

Using a three-step process, LiHMDS - H_2O - TMB, linear growth with a growth per cycle (GPC) of 0.4 Å was observed at a deposition temperature of 250°C (figure 1a) (red), although with an initial inhibited growth of nearly 100 cycles. While the reason for this delay was not further investigated, such inhibited growth regime is a common occurrence in ALD processes[7]. Similar growth behavior was observed throughout a deposition temperature between 125°C to 300°C, shown in figure 1b), with the GPC decreasing from respectively 0.5 Å to 0.35 Å . In decreasing the deposition temperature below 125°C, the condensation of a white powder was observed on the samples.

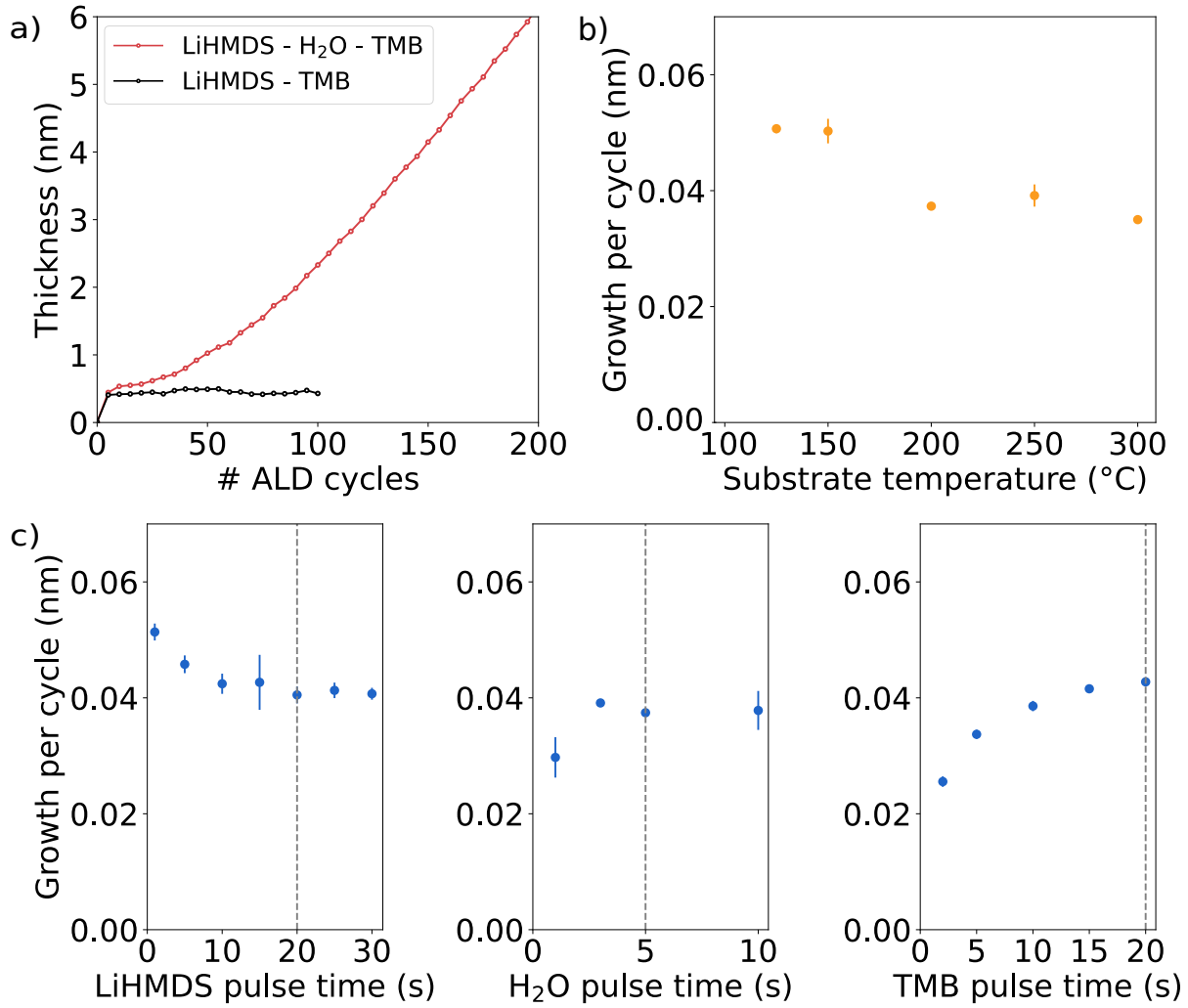

Figure 1: ALD characteristics for the LiHMDS-H_2O-TMB process. a) Linear growth at 250°C (red), compared to the process without water (black), where no growth is visible. b) Temperature window. c) From left to right: Saturation behavior of LiHMDS, H_2O and TMB at a deposition temperature of 250°C. All data are obtained from in-situ ellipsometry measurements on Si. Error bars in c) are obtained from repeated deposition experiments.

Focusing on the deposition temperature of 250°C, it can be seen that saturated ALD growth is observed for all precursors, figure 1c). It can be seen, however, that the saturation of LiHMDS deviates from conventional saturation behavior with an initially high GPC which decreases for longer dosing time. This effect has been reported by Kukli et al[27] for the LaHMDS and H_2O process. They suggested that the decrease in growth is related to partial passivation of the growing film due to inert $SiMe_3$ surface sites formation from byproduct reactions with

available -OH groups. Here, the GPC variation remains small, and it is expected that the surface passivation by Si incorporation will be minimal. Saturation of H_2O occurs quickly, whereas TMB requires a longer saturation time, hinting at a slow reaction with available -OH groups. For the continuation of this work, we established optimal conditions with pulse times of 20 s for LiHMDS, 5 s for H_2O and 20 s for TMB.

3.1.2 Thin film characterization

After optimization of the growth conditions, the composition and chemical state at different deposition temperatures (125°C, 250°C and 300°C) were analyzed.

Composition - To study the composition of each material, 60 nm thick films were deposited on a Si substrate with native oxide for ERD analysis. As shown in table 1, the film deposited at 125°C consists out of 23.5 at.% Li, 22.2 at.% B and 48.8 at.% O. Previous attempts to produce other metal borates using TMB, such as aluminium borates, resulted in a low B incorporation, typically below 10 at.%[15,28], while in our films a higher B content is achieved. The B/O ratio of 0.45 and the Li/B ratio of 1.06 at 125°C, closely resembles the known structure of lithium metaborate ($LiBO_2$), which has a B/O ratio of 0.5 and a Li/B ratio of 1. As the deposition temperature increases, the B content remains relatively stable, while the Li/B ratio and B/O ratio increase to 1.37 and 0.53 respectively, at 300°C. At higher temperatures, the deposited lithium borate is likely a mixture of $LiBO_2$ and the slightly more lithium-rich $Li_6B_4O_9$, as the Li/B and B/O values fall between those of the individual compounds. Although the exact reason for more lithium incorporation is not clear, it could indicate alternative reaction pathways and/or partial decomposition of the LiHMDS precursor at elevated temperatures.

It should be noted that C, Si, N and H contamination is observed in the films, with levels increasing alongside the substrate temperature. This rise in contamination, combined

with the increasing lithium concentration, suggests partial, but limited, decomposition of the LiHMDS precursor at elevated temperature. While most contaminant levels are relatively similar to those reported in literature related to other HMDS-precursors in thermal ALD processes, the nitrogen contamination at temperatures above 250°C is notably different[7,24,26,27,29,30], reaching almost 5 at.% at 250°C and 300°C and homogeneously distributed throughout the films (figure S1).

Table 1: ERD composition of lithium borate thin films deposited at 125°C, 250°C and 300°C. The ERD depth profiles are shown in figure S1.

T (°C)	Li (at.%)	B (at.%)	O (at.%)	C (at. %)	Si (at. %)	N (at. %)	H (at. %)
125	23.5	22.2	48.8	1.0	0.4	0.1	3.9
250	27.8	19.5	41.1	0.7	1.1	4.5	5.3
300	28.3	20.7	38.9	1.2	0.7	4.9	5.4

Chemical structure - In order to investigate the chemical structure, 15 nm films were deposited and transferred without air-exposure from an Ar-filled glovebox to the UHV-XPS chamber. High-resolution scans with a pass energy of 50 eV were made to ensure proper peak fitting. As all materials showed large amounts of adventitious carbon ($>$ 20 at.%) and traces of Li_2CO_3 at the surface, the analysis of the chemical state of the lithium borates was performed after sputtering. All data shown in figure 2 are after 400s of Ar^+ ion sputtering with a low beam energy of 500 eV, in order to minimize the sputter damage of the thin films. Since we have sputtered only $\sim$1 nm of material, carbon is still present ($\sim$10 at.%), but the C 1s signal quickly disappears with continuous sputtering (figure S2).

The Li 1s spectra, in figure 2, show a Li peak at $\sim$55 eV, which corresponds closely with the reported value of 55.2 eV[31]. The B 1s spectra show a broad peak at 191.5 - 191.2 eV, characteristic of a lithium borate structure[31]. The O 1s spectra can be fitted with 2 peaks. Based on prior experimental[6,31] and computational[32] studies on lithiated borates,

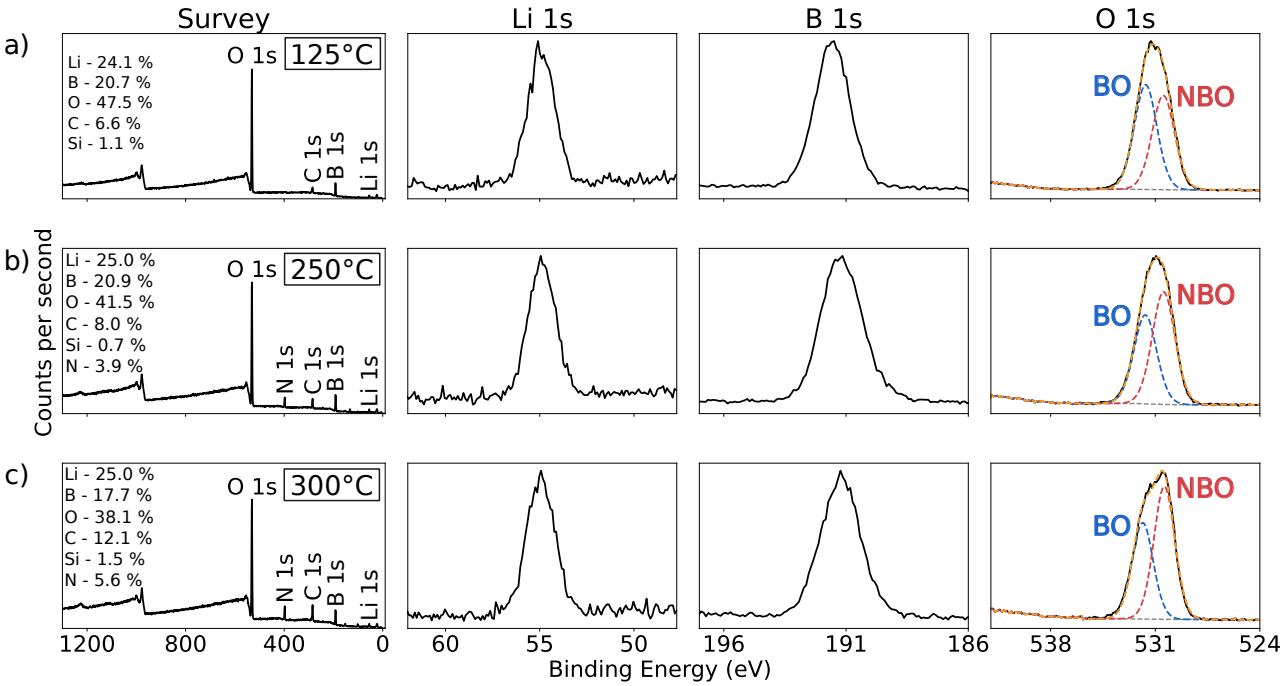

Figure 2: XPS spectra for the lithium borate process at deposition temperatures of a) 125°C, b) 250°C and c) 300°C. The O 1s spectrum can be divided into 2 peaks which correspond with bridging oxygen atoms at ∼531.7 eV (blue) and non-bridging oxygen atoms at 530.4 eV (red). All data shown are after 400s of sputtering with an Ar^+ ion beam energy of 500 eV. Note: Si is not indicated in the survey spectra for space and readability.

these peaks can be attributed to structures with bridging oxygen atoms (BO) at ∼531.7 eV (blue) and structures with non-bridging oxygen atoms (NBO) at 530.4 eV (red), consistent with previous lithium borate XPS studies[6,31]. The NBO:BO ratio increases from 0.9 at 125°C to 1.4 at 300°C, indicating higher NBO contribution, which could be important as this has been shown to impact ionic conductivity[32].

Crystallinity - The same batch of samples used for ERD analysis was subjected to XRD measurements. At all deposition temperatures, the lithium borate thin films were amorphous as-deposited. (Deposition temperatures 125°C and 250°C can be found in figure S3, deposition temperature 300°C in figure 5c).)

Ionic Conductivity - From the above section, we have demonstrated the ability to pro-

duce lithium borates with minimal contamination at low temperatures. As the deposition temperature increases, both the lithium content and contamination level rise. To investigate the influence of deposition temperature on the electrochemical properties, we focused on the films deposited at 125°C and 250°C.

Through-plane impedance spectroscopy was used to obtain the ionic conductivity of lithium borate films deposited at 125°C and 250°C. A Pt/80 nm lithium borate/Pt structure was used, where the Pt top electrode consists of sputtered dots of varying size. Samples were deposited in an ALD and PVD reactor connected to a glovebox and transported without air exposure for electrochemical measurements. Nyquist plots with a semicircle at high frequencies and a tail in the lower frequency region were obtained for both deposition temperatures (figure 3a) and b)). The equivalent circuit that could be fitted to these spectra is $R_0(R_1Q_1)Q_2$, where the brackets indicate a parallel circuit. The first in-series resistance R_0 can be attributed to the resistance of the cables. The resistance R_1 in parallel to a constant phase element Q_1 can be assigned to the bulk resistivity against the diffusion of Li-ions and the constant phase element Q_2 in series corresponds to the charge build-up at the interface of the electrode[33].

The ionic conductivity can be calculated according to the formula:

$$\sigma = \frac{t}{R_1 A} \tag{1}$$

where t is the thickness of the deposited film, R_1 is the value of the parallel resistance obtained from the fit and A is the area of the sputtered dots. During the measurements the samples were heated from 30°C until 60°C, as shown in figure 3a) and b). At elevated temperatures, the diameter of the semicircle decreases, which corresponds to a lower resistance R_1 and, consequently, a higher ionic conductivity. This observation aligns with the Arrhenius

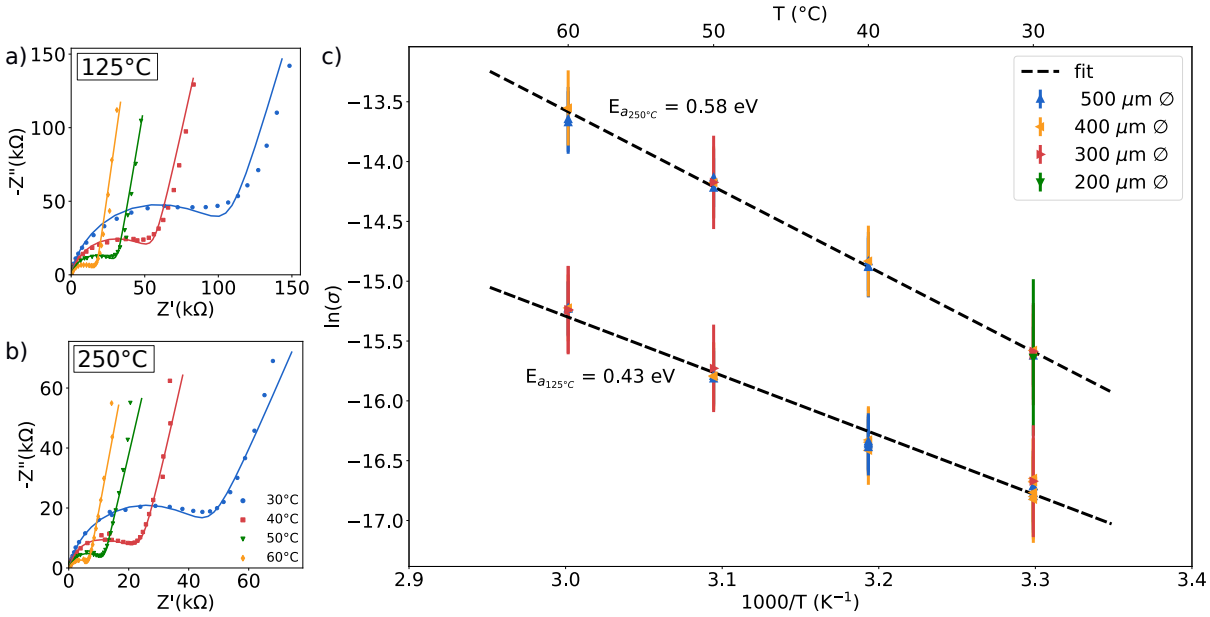

Figure 3: a) and b) Nyquist plots for lithium borate deposited at 125°C and 250°C, respectively. For each sample, the temperature was increased from 30°C to 60°C in steps of 10°C. At each temperature, multiple spectra were taken. For each measurement, the conductivity σ is calculated from the fitted parallel resistance R_1. This can be plotted as a function of 1000/T. c) From the slope of the fit through these points, the activation energy can be calculated. 80 nm thick films were deposited.

equation:

$$\sigma = \sigma_0 \cdot \exp(\frac{-E_a}{kT}) \tag{2}$$

with σ_0 the preexponential factor, k the Boltzmann constant, E_a the activation energy and T the absolute temperature. By plotting the logarithm of the calculated conductivity values for different dot sizes and temperatures as a function of (1000/T), the Arrhenius equation can be fitted to these points, as shown in figure 3c). The slope of this fit allows us to calculate the activation energy E_a. Using the obtained activation energies, the conductivity values can be extrapolated to room temperature. The lithium borate deposited at 125°C has an ionic conductivity of 3.92 x 10^{-8} S cm^{-1} at 25°C with an activation energy of 0.43 ± 0.04 eV. At a deposition temperature of 250°C, a more conductive film is obtained, with a conductivity of 1.17 x 10^{-7} S cm^{-1} at 25°C and an activation energy of 0.58 ± 0.01 eV.

A possible explanation for the increased activation energy could be found in the amount of NBO to BO. According to the model introduced by Anderson and Stuart[34], the activation energy is the sum of the binding energy (E_b, the energy required to move an ion) and the strain energy (E_s, the energy required to distort the surrounding structure). As reported by Martin[35], an increase in the amount of NBOs can be related to an increase in E_b. As more NBOs are introduced in the system, more anionic charge is localized on these oxygen atoms, which imposes a larger Coulombic electrostatic force on the Li-ions. Thus, even though a more disconnected structure enhances the mobility, it can also increase the energy required for motion.

Despite the higher activation energy, the lithium borate deposited at 250°C exhibits higher overall ionic conductivity. Based on the above discussion, one possible explanation could be attributed to an increase in the pre-exponential factor σ_0 in the Arrhenius equation (equation 2). The stronger electrostatic interactions between Li^+ ions and NBOs directly influence the vibration force constant, which leads to a higher frequency of Li^+ jump attempts. Since σ_0 is proportional to the jump-attempt frequency, a higher σ_0 could potentially contribute to a higher ionic conductivity[35].

Figure 4 summarizes the Li-containing ALD materials reported in the literature. Certain materials, like LiPON and Li_3BO_3-Li_2CO_3, still demonstrate superior ionic conductivities compared to the lithium borate in this work. These materials achieve higher conductivities because they are doped with nitrogen (N) or carbon (C), which influences their structure and enhances their ionic transport properties[6,36,37]. Similarly, the higher ionic conductivity observed for the lithium borate deposited at 250°C may also be partially influenced by the increased N incorporation. While this work demonstrates an ALD lithium borate with very good ionic conductivity, exploring the effects of doping remains a promising avenue for further improvement.

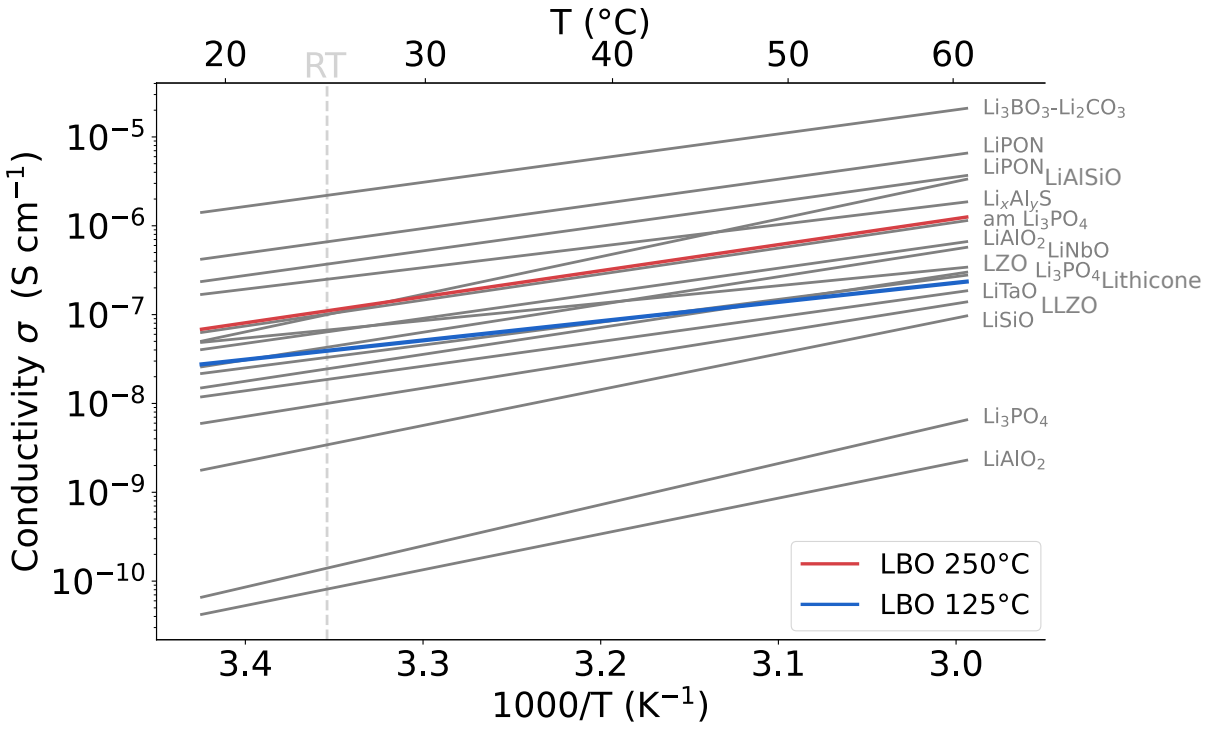

Figure 4: Reported ionic conductivity values for Li-containing ALD films. References from high to lower σ-value at RT: Li_3BO_3 - $Li2CO_3$[6], LiPON (LiHMDS - DEPA)[36], LiPON (LiO^tBu - DEPA)[37], Li_xAl_yS[38], amorphous Li_3PO_4[7], LiAlSiO[39], LZO (Li_3ZrO_3)[9], LiAlO[8], LiNbO[40], Lithicone[41], Li_3PO_4 (LiO^tBu)[42], LiTaO[43], LLZO[44], LiSiO[45], Li_3PO_4 (LiHMDS)[33], LiAlO[10]. Adapted from[7]. Copyright 2022 The Royal Society of Chemistry.

3.2 The Effect of Phosphorus Incorporation in Lithium Borates

Since the electrochemical performance of lithium borophosphate materials depends on the composition[17,18], we investigated how the incorporation of P into the lithium borate affects the electrochemical properties of the film. In an attempt to achieve different lithium borophosphate (LBPO) thin film compositions, a supercycle approach was used in which the newly developed ALD process for lithium borates (LBO) and the existing ALD process for lithium phosphates[24] (LPO) were combined. The number of LPO subcycles (l) was varied relative to the number of LBO subcycles (k). The cycle ratio (CR) for LBO is defined as CR_{LBO} = k / (k + l) and will be used in the discussion below. A CR_{LBO} equal to 1 represents a pure lithium borate, whereas a CR_{LBO} of 0 represents a pure LPO. In this work, we studied the following CR_{LBO} values, 1, 0.5 (k=1, l=1), 0.17 (k=1, l=5), 0.09 (k=1, l=10)

and 0. We indeed focused on low values for CR_{LBO} since literature indicates that the most significant changes in electrochemical properties occur for a lower borate incorporation[17,18]. A CR $\ll 0.5$ resembles doped materials[20], so we included both an extremely low B doping level (CR = 0.09) and a moderately low level (CR = 0.17). Additionally, CR = 0.5 was included to investigate a potential homogeneous LBPO material.

3.2.1 Process development and thin film characterization

The LiHMDS - TMP ALD process for lithium phosphates shows proper film growth only between 275°C and 325°C[24], therefor, a deposition temperature of 300°C was chosen for the deposition of the LBPO thin films during this work. At 300°C, a saturated GPC for LPO of 0.7 Å and according to ERD data, an $Li_{2.7}PO_{3.9}$ composition was obtained, which is in agreement with the work of Hämäläinen et al[24].

According to the rule of mixtures, the growth per supercycle should be a weighted average of the GPCs of the individual processes[20]. Figure 5a) shows that the GPC for different CR_{LBO} values lies between 0.6 Å and 0.5Å , with a general downwards trend, however slightly deviating from what is expected. This deviation suggests that interactions between the LBO and LPO processes might be affecting the growth rates in a more complex manner than a simple weighted average would predict.

Composition - ERD data of 60 nm films for different cycle ratios are summarized in table 2. For all cycle ratios, both B and P were successfully incorporated. At low cycle ratios, a B-doped Li_3PO_4 material is obtained, whereas at higher CR_{LBO}, a more B-rich material is observed. Since the change in B and P incorporation is not linear, we simulated the expected composition using the rule of mixtures[20] with the following equation:

$$\text{fraction of LBO} = \frac{\rho_{LBO} \cdot GPC_{LBO} \cdot CR_{LBO}}{(\rho_{LBO} \cdot GPC_{LBO} \cdot CR_{LBO}) + (\rho_{LPO} \cdot GPC_{LPO} \cdot CR_{LPO})} \tag{3}$$

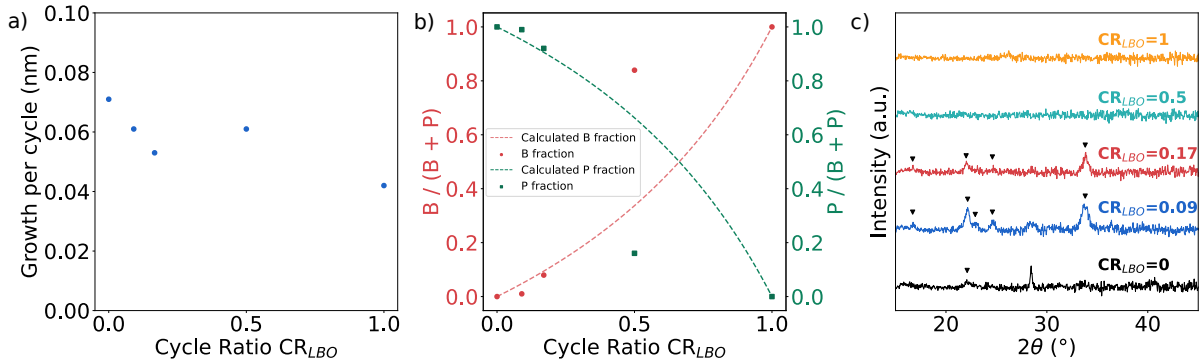

Figure 5: a) GPC values as a function of the cycle ratio, obtained with in-situ ellipsometry on Si substrate. b) The measured B fraction (red) and P fraction (green), together with the calculated values in dashed lines. c) XRD data of the as-deposited samples, with the markers indicating the peaks corresponding to a crystalline Li_3PO_4 structure[46]. Lower CR values correspond to a lower amount of lithium borate subcycles ($CR_{LBO} = 1$: lithium borate, $CR_{LBO} = 0$: lithium phosphate).

where $\rho_{LBO} \approx 2.1$ g/cm^3 and $\rho_{LPO} \approx 2.5$ g/cm^3 represent the densities of the deposited LBO and Li_3PO_4, as determined by X-ray reflectivity measurements. As shown in figure 5b), low CR_{LBO} values follow this rule, indicating that the amount of B incorporation in the material is as expected. However, at $CR_{LBO} = 0.5$, the measured atomic percentages were 13.6% for B and only 2.6 at.% of P, despite expecting nearly equal B and P content of about 7 at.%.

The non-linear behavior can possibly be explained by the nucleation delays between the LBO and LPO processes. In an experiment where a lithium borate film was grown and monitored using in-situ ellipsometry after each subcycle (figure S4), significant nucleation delays were observed for the LiHMDS - TMP process when deposited on top of the lithium borate surface. This could explain the unexpectedly low P incorporation with increasing LBO subcycles (e.g. with a CR_{LBO} of 0.5), as the more frequent LBO cycles disrupt LPO growth. The complex interplay of nucleation effects between the LPO and LBO processes, along with the low reactivity of TMP and TMB, likely cause the composition and GPC of the mixed lithium borophosphate films to deviate from the expected rule of mixtures.

Additionally, the ERD data also reveal that combining the LBO and LPO cycles results in

a decrease of C contamination as the CR_{LBO} increases. This suggests that more frequent LBO cycles or H_2O steps, corresponding to higher CR_{LBO} values, play a role in reducing the C contamination. We propose that the H_2O step removes physisorbed LiHMDS/HMDS to form hydroxyl groups, and also removes residual methyl groups from the TMP molecule. Supporting this, in-situ ellipsometry data show that H_2O significantly decreases the thickness of the deposited material (figure S4). It would be interesting to investigate whether an intermediate H_2O pulse within the LiHMDS-TMP process could similarly reduce C contamination; however, this is beyond the scope of the present study.

Table 2: ERD composition for different values of the CR_{LBO}. Lower CR values correspond to a lower amount of lithium borate subcycles ($CR_{LBO} = 1$: lithium borate, $CR_{LBO} = 0$: lithium phosphate). The ERD depth profiles are shown in figure S5.

CR_{LBO}	Li (at.%)	B (at.%)	P (at.%)	O (at.%)	C (at.%)	Si (at.%)	N (at.%)	H (at.%)
1	28.3	20.7	-	38.9	1.2	0.7	4.9	5.4
0.5	27.5	13.6	2.6	41.1	2	1	3.9	8.3
0.17	28.7	0.9	10.4	43.9	4.5	0.6	0.6	10.3
0.09	29.7	0.1	9.8	45.5	4.4	-	0.3	10.2
0	28.7	-	10.5	40.4	9.3	0.5	0.7	9.9

Crystallinity - The same samples deposited for ERD analysis were also used for XRD measurements. At 300°C, the LiHMDS - TMP results in a crystalline Li_3PO_4 structure, shown in figure 5c). Interestingly, the LBPO thin film with a B doping of 0.1 at.% and 0.9 at.% result in a more crystalline structure than the pure LPO. Further increasing the B doping decreases the crystallinity until the films become entirely amorphous. This is opposite to what Werbrouck et al[7] have reported as they doped Li_3PO_4 with 1 at.% of Al by using the LiHMDS - TMA - TMP process, which resulted in an amorphous lithium phosphate. A possible explanation for a more crystalline film in the case when mixing with borates could be found in the amount of carbon impurities being present in the doped film. For the case of the amorphous Li_3PO_4 by Al doping, the C doubled in amount with regard to the original

deposition process. In our case, the C decreases by half, from 9.3 at.% to 4.4 at.%. Furthermore, a report on ALD of TiO_2 has shown that fewer C impurities lower the crystallization temperature[47]. This is an interesting result, as it allows to control the crystallinity of Li_3PO_4.

Influence on the electrochemical performance - To evaluate the electrochemical performance of both the pure and mixed coatings on cathode materials, planar $LiMn_2O_4$[21] was selected as a model system, on which 10 nm LBPO coatings were deposited. The thicknesses of the coatings were determined via in-situ ellipsometry on a Si substrate placed next to the $LiMn_2O_4$ substrate in the ALD reactor. The electrodes were cycled between 3.5 V and 4.5 V vs Li^+/Li, where both the uncoated and coated samples displayed the characteristic peak pair in the 4.0 V vs Li^+/Li region, as shown in figure 6a). This indicates that the LBPO coatings do not exhibit a severe blocking nature, unlike Al_2O_3, where even a 1 nm layer can suppress electrochemical activity[48]. While there is minimal variation in peak current and position between the uncoated and coated samples, the coated electrodes with higher CR_{LBO} values (B-rich coatings) display slightly sharper peaks, suggesting improved electrochemical kinetics compared to the uncoated electrodes.

However, the C-rate performance, as seen in figure 6b), shows that at 1C, the capacity of the coated samples remains comparable to the uncoated $LiMn_2O_4$. Above 5C, the capacity of the P-rich coatings declines more rapidly than that of the uncoated $LiMn_2O_4$, while the B-rich coatings maintain similar capacity to the uncoated material up to 100C.

There appears to be an optimal value in B/P ratio, with the lithium borate containing a small amount of P ($CR_{LBO} = 0.5$) showing the best coating kinetics. It is important to note that protective coatings on 3D electrode particles typically require only a few ALD cycles in order to maintain ionic conductivity and ensure optimal electrochemical performance[3]. In this work, however, relatively thick 10 nm coatings were used to better observe the effect

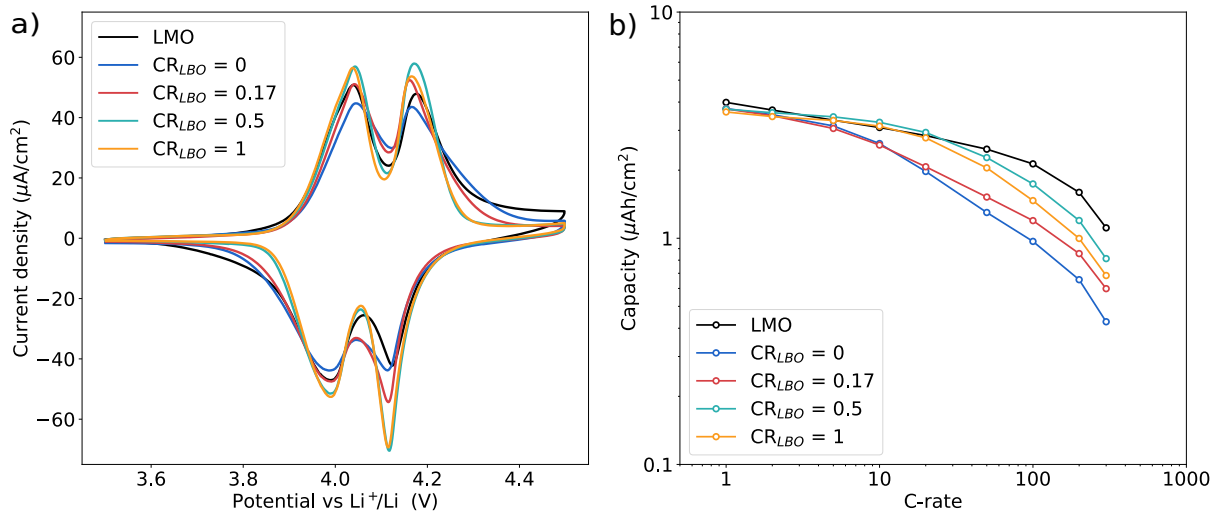

Figure 6: Electrochemical performance of the uncoated and 10 nm ALD coated $LiMn_2O_4$ electrodes. a) Cyclic voltammogram cycled between 3.5 V and 4.5 V vs Li^+/Li at a scan rate of 1 mV/s. b) Lithiation capacity densities at different C-rates, cycled between 3.5 V and 4.5 V vs Li^+/Li with a current density of 6 $\mu A/cm^2$ corresponding to 1C. ($CR_{LBO} = 1$: lithium borate, $CR_{LBO} = 0$: lithium phosphate)

of the layers on the electrochemical properties, making comparisons among ALD coatings easier. While the coating thickness may contribute to the lower capacity values observed at higher C-rates, they do not significantly impede Li-ion transport, as the visible $LiMn_2O_4$ peak pair suggests. This is, as mentioned earlier, already a significant improvement over the kinetics of the typical inert coatings proposed in current literature. Further optimization of the coating thickness could still improve both the kinetics and the overall performance of the coated electrodes[48].

To study the protection against cathode-electrolyte interphase formation at elevated potentials more in-depth, 10 nm coatings were deposited on Pt substrates and cycled up to 6 V vs Li^+/Li. Carbonate-based electrolytes, such as PC, decompose at potentials above 4 V vs Li^+/Li, which can be seen in figure 7, where an increase in current density is visible for the uncoated Pt electrode from 4.1 V vs Li^+/Li. This increase in current density corresponds to the onset of electrolyte breakdown, which forms a decomposition layer on top of the cathode, degrading the electrode's performance. When an LBPO coating is applied, the increase in

current density is significantly reduced and the onset of decomposition is shifted to higher potential values, indicating enhanced protection. The pure lithium borate coating provides the best stability, showing no increase in current density up to 6 V vs Li^+/Li. On the other hand, materials with higher P content (CR_{LBO} = 0, 0.09 and 0.17) exhibit slightly reduced stability with decreasing CR_{LBO} value in comparison with the pure lithium borate. This could be due to changes in crystallinity or compositional variations and contamination.

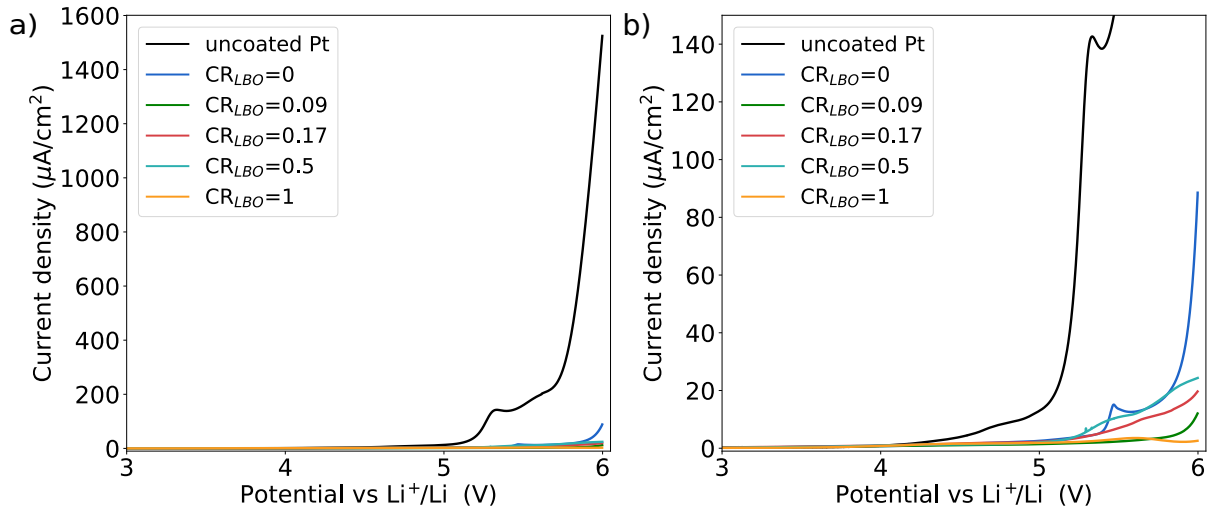

Figure 7: Stability of the uncoated and 10 nm ALD coated Pt electrodes. The cells were cycled from OCP value to 6 V vs Li^+/Li at a scan rate of 1 mV/s, with figure b) a zoomed-in version of figure a). (CR_{LBO} = 1: lithium borate, CR_{LBO} = 0: lithium phosphate)

Based on the above results, it appears that the performance of the lithium borate coating can be altered by incorporating P into the borate structure. The addition of a small amount of P (CR_{LBO} = 0.5) offers the most optimal coating kinetics when a 10 nm coating is used, and significantly suppresses the cathode-electrolyte interphase formation at elevated potentials. It should be noted that electrochemical stability measurements were performed at room temperature. Phosphate materials have a very good thermal stability[5], so more research should be conducted to investigate the stability at elevated temperatures. It could for example be that, while the kinetics of the coating slightly decrease with increasing P content, the stability at elevated temperatures might be significantly improved. Overall,

these findings highlight that lithium borophosphate materials provide excellent protection at elevated potentials and, combined with their promising kinetic performance, demonstrate potential for use as artificial interfacial layers in advanced battery systems.

4 Conclusion

In this work, we successfully developed a novel ALD process for lithium borate materials. The three-step process, LiHMDS - H_2O - TMB, results in linear growth with a GPC of ~0.4 Å. We demonstrated that the deposition temperature influences both the composition and ionic conductivity of the films. At all temperatures, LBO was deposited with minimal carbon contamination (~1 at.%). Higher deposition temperatures led to increased lithium content and a higher NBO:BO ratio, and an enhanced ionic conductivity, reaching 1.17 x 10^{-7} S/cm at 25°C for a lithium borate deposited at 250°C. Additionally, we combined the lithium borate process with a lithium phosphate ALD process to study the influence of P incorporation. Notably, we observed considerable deviations from the standard rule of mixtures, likely linked to a nucleation delay of lithium phosphate on a lithium borate surface. Furthermore, an impact on the crystallinity was observed at low levels of B-doping in Li_3PO_4. Pure lithium phosphate was less crystalline compared to B-doped lithium phosphates, likely due to reduced C contamination. Finally, we demonstrated the effectiveness of these materials as interfacial layers for lithium-ion battery cathodes, showing only very limited hindrance to Li-ion transport in a $LiMn_2O_4$ model system using 10 nm thick (mixed) coatings, with stability maintained up to 6 V. These results highlight the potential of these lithium borophosphate coatings as promising interfacial layers for next-generation batteries, providing improved stability and preserving overall performance.

5 Acknowledgments

The authors acknowledge the financial support from the UGENT-GOA-01G02124 project and thank Fonds Wetenschappelijk Onderzoek - Vlaanderen (FWO) for providing Tippi Verhelle with an SB grant (1SH9024N). Lowie Henderick acknowledges the FWO for a junior postdoctoral fellowship (1254324N).

6 Supporting Information description

ERD depth profiles of lithium borate deposited at 125°C, 250°C and 300°C; XPS spectra of C 1s after sputtering for lithium borate deposited films 300°C; XRD patterns for lithium borate deposited at 125°C and 250°C; Nucleation behavior of lithium phosphate on a lithium borate surface, measured with in-situ ellipsometry; In-situ ellipsometry after each precursor exposure; ERD depth profiles of the different obtained lithium borophosphates with CR_{LBO} = 0, 0.09, 0.17 and 0.5.

References

(1) Goodenough, J. B.; Kim, Y. Challenges for Rechargeable Li Batteries. *Chemistry of Materials* **2010**, *22*, 587–603.

(2) Wu, J.; Shen, L.; Zhang, Z.; Liu, G.; Wang, Z.; Zhou, D.; Wan, H.; Xu, X.; Yao, X. All-Solid-State Lithium Batteries with Sulfide Electrolytes and Oxide Cathodes. *Electrochemical Energy Reviews* **2021**, *4*, 101–135.

(3) Jung, Y. S.; Cavanagh, A. S.; Dillon, A. C.; Groner, M. D.; George, S. M.; Lee, S.-H. Enhanced Stability of $LiCoO_2$ Cathodes in Lithium-Ion Batteries Using Surface Modification by Atomic Layer Deposition. *Journal of The Electrochemical Society* **2009**, *157*, A75.

(4) Cheng, H.-M.; Wang, F.-M.; Chu, J. P.; Santhanam, R.; Rick, J.; Lo, S.-C. Enhanced Cycleabity in Lithium Ion Batteries: Resulting from Atomic Layer Depostion of Al_2O_3 or TiO_2 on $LiCoO_2$ Electrodes. *The Journal of Physical Chemistry C* **2012**, *116*, 7629–7637.

(5) Henderick, L.; Dhara, A.; Werbrouck, A.; Dendooven, J.; Detavernier, C. Atomic layer deposition of metal phosphates. *Applied Physics Reviews* **2022**, *9*, 011310.

(6) Kazyak, E.; Chen, K.-H.; Davis, A. L.; Yu, S.; Sanchez, A. J.; Lasso, J.; Bielinski, A. R.; Thompson, T.; Sakamoto, J.; Siegel, D. J.; Dasgupta, N. P. Atomic layer deposition and first principles modeling of glassy Li_3BO_3–Li_2CO_3 electrolytes for solid-state Li metal batteries. *J. Mater. Chem. A* **2018**, *6*, 19425–19437.

(7) Werbrouck, A.; Mattelaer, F.; Dhara, A.; Nisula, M.; Minjauw, M.; Munnik, F.; Dendooven, J.; Detavernier, C. Surface reactions between LiHMDS, TMA and TMP leading to deposition of amorphous lithium phosphate. *J. Mater. Chem. A* **2022**, *10*, 3543–3551.

(8) Park, J. S.; Meng, X.; Elam, J. W.; Hao, S.; Wolverton, C.; Kim, C.; Cabana, J. Ultrathin Lithium-Ion Conducting Coatings for Increased Interfacial Stability in High Voltage Lithium-Ion Batteries. *Chemistry of Materials* **2014**, *26*, 3128–3134.

(9) Zhao, F. et al. Tuning bifunctional interface for advanced sulfide-based all-solid-state batteries. *Energy Storage Materials* **2020**, *33*, 139–146.

(10) Hu, Y.; Ruud, A.; Miikkulainen, V.; Norby, T.; Nilsen, O.; Fjellvåg, H. Electrical characterization of amorphous $LiAlO_2$ thin films deposited by atomic layer deposition. *RSC Adv.* **2016**, *6*, 60479–60486.

(11) Liu, Z.; Chai, J.; Xu, G.; Wang, Q.; Cui, G. Functional lithium borate salts and their potential application in high performance lithium batteries. *Coordination Chemistry Reviews* **2015**, *292*, 56–73.

(12) Hu, W.; Zhang, C.; Jiang, H.; Zheng, M.; Wu, Q.-H.; Dong, Q. Improving the electrochemistry performance of layer $LiNi_{0.5}Mn_{0.3}Co_{0.2}O_2$ material at 4.5V cutoff potential using lithium metaborate. *Electrochimica Acta* **2017**, *243*, 105–111.

(13) Wang, D.; Li, X.; Wang, Z.; Guo, H.; Chen, X.; Zheng, X.; Xu, Y.; Ru, J. Multifunctional Li_2O-$2B_2O_3$ coating for enhancing high voltage electrochemical performances and thermal stability of layered structured $LiNi_{0.5}Co_{0.2}Mn_{0.3}O_2$ cathode materials for lithium ion batteries. *Electrochimica Acta* **2015**, *174*, 1225–1233.

(14) Park, N. R.; Li, Y.; Yao, W.; Zhang, M.; Han, B.; Mejia, C.; Sayahpour, B.; Shimizu, R.; Bhamwala, B.; Dang, B.; Kumakura, S.; Li, W.; Meng, Y. S. Understanding the Role of Lithium Borate as the Surface Coating on High Voltage Single Crystal $LiNi_{0.5}Mn_{1.5}O_4$. *Advanced Functional Materials* **2024**, *34*, 2312091.

(15) Mattelaer, F.; Van Daele, M.; Minjauw, M. M.; Nisula, M.; Elliott, S. D.; Sajavaara, T.; Dendooven, J.; Detavernier, C. Atomic Layer Deposition of Localized Boron- and

Hydrogen-Doped Aluminum Oxide Using Trimethyl Borate as a Dopant Precursor. *Chemistry of Materials* **2020**, *32*, 4152–4165.

(16) Li, J.; Xiang, J.; Yi, G.; Hu, Z.; Liu, X.; Chen, R. Stabilization of the surface and lattice structure for $LiNi_{0.83}Co_{0.12}Mn_{0.05}O_2$ via B_2O_3 atomic layer deposition and post-annealing. *Energy Adv.* **2024**, *3*, 1688–1696.

(17) Magistris, A.; Chiodelli, G.; Villa, M. Lithium borophosphate vitreous electrolytes. *Journal of Power Sources* **1985**, *14*, 87–91.

(18) Larink, D.; Eckert, H.; Reichert, M.; Martin, S. W. Mixed Network Former Effect in Ion-Conducting Alkali Borophosphate Glasses: Structure/Property Correlations in the System $[M_2O]_{1/3}[(B_2O_3)_x(P_2O_5)_{1-x}]_{2/3}$ (M = Li, K, Cs). *The Journal of Physical Chemistry C* **2012**, *116*, 26162–26176.

(19) Ji, Y. J.; Noh, S.; Seong, J. Y.; Lee, S.; Park, Y. J. Li_3BO_3-Li_3PO_4 Composites for Efficient Buffer Layer of Sulphide-Based All-Solid-State Batteries. *Batteries* **2023**, *9*, 292.

(20) Mackus, A. J. M.; Schneider, J. R.; MacIsaac, C.; Baker, J. G.; Bent, S. F. Synthesis of Doped, Ternary, and Quaternary Materials by Atomic Layer Deposition: A Review. *Chemistry of Materials* **2019**, *31*, 1142–1183.

(21) De Taeye, L. L.; Vereecken, P. M. Chemo-mechanical effect of chlorine modified TiO2 coatings on LMO. *J. Mater. Chem. A* **2022**, *10*, 24398–24409.

(22) Fairley, N.; Fernandez, V.; Richard-Plouet, M.; Guillot-Deudon, C.; Walton, J.; Smith, E.; Flahaut, D.; Greiner, M.; Biesinger, M.; Tougaard, S.; Morgan, D.; Baltrusaitis, J. Systematic and collaborative approach to problem solving using X-ray photoelectron spectroscopy. *Applied Surface Science Advances* **2021**, *5*, 100112.

(23) Dobbelaere, T.; Vereecken, P. M.; Detavernier, C. A USB-controlled potentiostat/galvanostat for thin-film battery characterization. *HardwareX* **2017**, *2*, 34–49.

(24) Hämäläinen, J.; Holopainen, J.; Munnik, F.; Hatanpää, T.; Heikkilä, M.; Ritala, M.; Leskelä, M. Lithium Phosphate Thin Films Grown by Atomic Layer Deposition. *Journal of The Electrochemical Society* **2012**, *159*, A259.

(25) Werbrouck, A.; Mattelaer, F.; Minjauw, M.; Nisula, M.; Julin, J.; Munnik, F.; Dendooven, J.; Detavernier, C. Reaction Pathways for Atomic Layer Deposition with Lithium Hexamethyl Disilazide, Trimethyl Phosphate, and Oxygen Plasma. *The Journal of Physical Chemistry C* **2020**, *124*, 27829–27839.

(26) Tomczak, Y.; Knapas, K.; Sundberg, M.; Leskelä, M.; Ritala, M. In Situ Reaction Mechanism Studies on Lithium Hexadimethyldisilazide and Ozone Atomic Layer Deposition Process for Lithium Silicate. *The Journal of Physical Chemistry C* **2013**, *117*, 14241–14246.

(27) Kukli, K.; Ritala, M.; Pore, V.; Leskelä, M.; Sajavaara, T.; Hegde, R.; Gilmer, D.; Tobin, P.; Jones, A.; Aspinall, H. Atomic Layer Deposition and Properties of Lanthanum Oxide and Lanthanum-Aluminum Oxide Films. *Chemical Vapor Deposition* **2006**, *12*, 158–164.

(28) Dhara, A.; Li, J.; Dendooven, J.; Detavernier, C. Strategies to produce boron-containing ALD thin films using trimethyl borate precursor: from thermal to plasma to combined-plasma approach. *AVS 22nd International Conference on Atomic Layer Deposition (ALD 2022), Abstracts* **2022**,

(29) Nam, W.-H.; Rhee, S.-W. Atomic Layer Deposition of ZrO_2 Thin Films Using Dichlorobis[bis-(trimethylsilyl)amido]zirconium and Water. *Chemical Vapor Deposition* **2004**, *10*, 201–205.

(30) Nam, W.-H.; Rhee, S.-W. Atomic Layer Deposition of Hafnium Silicate Thin Films Using $HfCl_2[N(SiMe_3)_2]_2$ andH_2O. *Electrochemical and Solid-State Letters* **2004**, *7*, C55.

(31) Hensley, D.; Garofalini, S. XPS investigation of lithium borate glass and the $Li/LiBO_2$ interface. *Applied Surface Science* **1994**, *81*, 331–339.

(32) Varsamis, C.-P. E.; Vegiri, A.; Kamitsos, E. I. Molecular dynamics investigation of lithium borate glasses: Local structure and ion dynamics. *Phys. Rev. B* **2002**, *65*, 104203.

(33) Put, B.; Mees, M. J.; Hornsveld, N.; Hollevoet, S.; Sepúlveda, A.; Vereecken, P. M.; Kessels, W. M. M.; Creatore, M. Plasma-Assisted ALD of LiPO(N) for Solid State Batteries. *Journal of The Electrochemical Society* **2019**, *166*, A1239.

(34) Anderson, O. L.; Stuart, D. A. Calculation of Activation Energy of Ionic Conductivity in Silica Glasses by Classical Methods. *Journal of the American Ceramic Society* **1954**, *37*, 573–580.

(35) Martin, S. W. Conductivity Activation Energy Relations in High-Sodium-Content Borate and Aluminoborate Glasses. *Journal of the American Ceramic Society* **1988**, *71*, 438–445.

(36) Nisula, M.; Shindo, Y.; Koga, H.; Karppinen, M. Atomic Layer Deposition of Lithium Phosphorus Oxynitride. *Chemistry of Materials* **2015**, *27*, 6987–6993.

(37) Pearse, A. J.; Schmitt, T. E.; Fuller, E. J.; El-Gabaly, F.; Lin, C.-F.; Gerasopoulos, K.; Kozen, A. C.; Talin, A. A.; Rubloff, G.; Gregorczyk, K. E. Nanoscale Solid State Batteries Enabled by Thermal Atomic Layer Deposition of a Lithium Polyphosphazene Solid State Electrolyte. *Chemistry of Materials* **2017**, *29*, 3740–3753.

(38) Cao, Y.; Meng, X.; Elam, J. W. Atomic Layer Deposition of Li_xAl_yS Solid-State Electrolytes for Stabilizing Lithium-Metal Anodes. *ChemElectroChem* **2016**, *3*, 858–863.

(39) Cho, J.; Kim, T.; Seegmiller, T.; Chang, J. P. Elucidating the Surface Reaction Mechanisms During Atomic Layer Deposition of $Li_xAl_ySi_zO$ by in Situ Fourier Transform Infrared Spectroscopy. *The Journal of Physical Chemistry C* **2016**, *120*, 11837–11846.

(40) Wang, B.; Zhao, Y.; Banis, M. N.; Sun, Q.; Adair, K. R.; Li, R.; Sham, T.-K.; Sun, X. Atomic Layer Deposition of Lithium Niobium Oxides as Potential Solid-State Electrolytes for Lithium-Ion Batteries. *ACS Applied Materials & Interfaces* **2018**, *10*, 1654–1661, PMID: 29219291.

(41) Kazyak, E.; Shin, M.; LePage, W. S.; Cho, T. H.; Dasgupta, N. P. Molecular layer deposition of Li-ion conducting "Lithicone" solid electrolytes. *Chem. Commun.* **2020**, *56*, 15537–15540.

(42) Wang, B.; Liu, J.; Sun, Q.; Li, R.; Sham, T.-K.; Sun, X. Atomic layer deposition of lithium phosphates as solid-state electrolytes for all-solid-state microbatteries. *Nanotechnology* **2014**, *25*, 504007.

(43) Liu, J.; Banis, M. N.; Li, X.; Lushington, A.; Cai, M.; Li, R.; Sham, T.-K.; Sun, X. Atomic Layer Deposition of Lithium Tantalate Solid-State Electrolytes. *The Journal of Physical Chemistry C* **2013**, *117*, 20260–20267.

(44) Kazyak, E.; Chen, K.-H.; Wood, K. N.; Davis, A. L.; Thompson, T.; Bielinski, A. R.; Sanchez, A. J.; Wang, X.; Wang, C.; Sakamoto, J.; Dasgupta, N. P. Atomic Layer Deposition of the Solid Electrolyte Garnet $Li_7La_3Zr_2O_{12}$. *Chemistry of Materials* **2017**, *29*, 3785–3792.

(45) Wang, B.; Liu, J.; Norouzi Banis, M.; Sun, Q.; Zhao, Y.; Li, R.; Sham, T.-K.; Sun, X. Atomic Layer Deposited Lithium Silicates as Solid-State Electrolytes for All-Solid-State Batteries. *ACS Applied Materials & Interfaces* **2017**, *9*, 31786–31793, PMID: 28749129.

(46) Zemann, J. Die Kristallstruktur von Lithiumphosphat, Li_3PO_4. *Acta Crystallographica* **1960**, *13*, 863–867.

(47) Xie, Q.; Musschoot, J.; Deduytsche, D.; Meirhaeghe, R. L. V.; Detavernier, C.; den Berghe, S. V.; Jiang, Y.-L.; Ru, G.-P.; Li, B.-Z.; Qu, X.-P. Growth Kinetics and Crystallization Behavior of TiO_2 Films Prepared by Plasma Enhanced Atomic Layer Deposition. *Journal of The Electrochemical Society* **2008**, *155*, H688.

(48) Mattelaer, F.; Vereecken, P. M.; Dendooven, J.; Detavernier, C. The Influence of Ultrathin Amorphous ALD Alumina and Titania on the Rate Capability of Anatase TiO_2 and $LiMn_2O_4$ Lithium Ion Battery Electrodes. *Advanced Materials Interfaces* **2017**, *4*, 1601237.

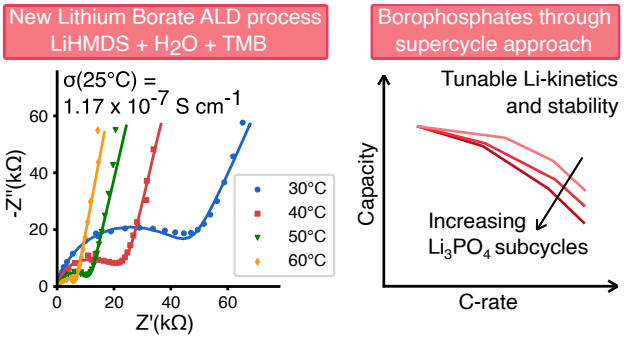
New Lithium Borate ALD process
LiHMDS + H2O + TMB
σ(25°C) =
1.17 x 10-7 S cm-1
-Z''(kΩ)
Z'(kΩ)
30°C
40°C
50°C
60°C
Borophosphates through
supercycle approach
Tunable Li-kinetics
and stability
Capacity
C-rate
Increasing
Li3PO4 subcycles

TOC Graphic